# Online dictionary learning for single-subject fMRI data unmixing

Argheesh Bhanot
*ICube UMR 7357, Université de Strasbourg, CNRS*
Strasbourg, France
argheesh.bhanot@etu.unistra.fr

Céline Meillier
*ICube UMR 7357, Université de Strasbourg, CNRS*
Strasbourg, France
meillier@unistra.fr

Fabrice Heitz
*ICube UMR 7357, Université de Strasbourg, CNRS*
Strasbourg, France
fabrice.heitz@unistra.fr

Laura Harsan
*ICube UMR 7357, Université de Strasbourg, CNRS*
Strasbourg, France
harsan@unistra.fr

***Abstract*—Independent component analysis (ICA) and dictionary learning (DL) methods are widely used to analyse resting state functional Magnetic Resonance Imaging (rs-fMRI) in multi-subject studies. These methods aim at decomposing the multi-subject data into common spatial abundance maps and their related temporal signatures.**

**We are interested here in such a decomposition for a *single-subject* rs-fMRI dataset. The above-mentioned methods often fail in this case because the problem becomes too ill-posed, requiring the use of additional prior information and the design of novel regularising constraints. The poor resolution of rs-fMRI data is an additional source of difficulty, yielding noisy and blurry spatial maps.**

**In this paper, we propose a new DL formulation adapted to the unique subject by integrating high-resolution (HR) spatial information to constrain single-subject data unmixing. HR information is provided by the registration of an anatomical atlas on the data set. We show on a quasi-real dataset from mice, the benefit of using an HR spatial segmentation map in the decomposition of low-resolution rs-fMRI.**

***Index Terms*—Dictionary Learning, resting state fMRI, single-subject rs-fMRI unmixing, high-resolution anatomical atlas.**

## I. Introduction

In recent years, resting state functional Magnetic Resonance Imaging (rs-fMRI) has been widely used for studying brain functional connectivity [1]. Rs-fMRI allows the observation of changes in cerebral activity by analysing the blood-oxygen-level-dependent (BOLD) signal [2]. At rest, only spontaneous activity is measured and a set of anatomical regions with the same fluctuations are considered part of a common network. A certain number of resting state networks have been examined in the mouse brain [3] and the human brain [1], [4]. Co-activation patterns are studied to determine the differences between healthy and pathological subjects using metrics such as correlation maps. Detecting precisely the different networks (localisation in the brain and temporal activity) is crucial for understanding a neurological disorder. In rs-fMRI, there is a compromise between the spatial resolution, and the temporal resolution which must be sufficiently fine to capture the networks activity fluctuations over time (these network activity fluctuations are called timecourses). As a consequence, rs-fMRI has a quite low spatial resolution, inducing a mixture of network contributions within the same voxel.

Unmixing timecourses linked to different networks leads to the following decomposition model:

$$\mathbf{Y} \simeq \mathbf{U}\mathbf{A}, \tag{1}$$

where $\mathbf{Y} \in \mathbb{R}^{N\times P}$ is the rs-fMRI data, $N$ is the length of timecourses , $P$ is the number of voxels in the brain, $\mathbf{U} \in \mathbb{R}^{N\times R}$ is the matrix containing the temporal signatures where $R$ is the number of components (networks). Matrix $\mathbf{A} \in \mathbb{R}^{R\times P}$ is the abundance matrix coding the fraction of the $R$ components contributions at each voxel. The estimation of $\mathbf{A}$ and $\mathbf{U}$ is a typical blind source separation problem. In neuroscience, spatial Independent Component Analysis (ICA) [5]–[7] has been extensively used to estimate a spatial basis $\mathbf{A}$, whose rows correspond to spatially independent sources, and the corresponding $\mathbf{U}$ matrix. Recently, DL methods have proven to be promising in rs-fMRI analysis [8]–[10]. They consist in seeking sparse spatial components instead of independent ones with a DL formulation:

$$\min_{\mathbf{A},\mathbf{U}} \ \frac{1}{2}\|\mathbf{Y} - \mathbf{U}\mathbf{A}\ \|_F^2 + \lambda||\mathbf{A}||_1. \tag{2}$$

This optimisation problem is not convex, but bi-convex and requires a good initialisation for $\mathbf{A}$ or $\mathbf{U}$ to obtain a relevant solution.

Methods for estimating spatial components and their temporal signatures are frequently used to conduct group analysis that aims at extracting networks expressed in a group of individuals. In group analysis, all the individuals are first registered to a common anatomical template. Registration to a template also allows the use of an associated atlas (anatomical segmentation map) to identify the anatomical regions involved in the different functional networks. This is particularly useful for identifying networks in ICA where the number of spatial components is difficult to set. Similarly, the atlas can be used to build a good initialisation of $\mathbf{A}$ in DL algorithms.

978-9-0827-9703-9/19/$31.00 

Detecting common networks through group analysis is obviously easier than single-subject analysis, because of the redundancy of information present in group data. In the single-subject case, the rs-fMRI data of a unique subject must be decomposed according to model (1). In this case, ill-posedness is even more pronounced than in group analysis, requiring additional prior information and regularisation.

In group analysis, registration of all individual fMRI-data to a common template requires the fMRI signals to be interpolated. This is detrimental to resolution and yields loss of information, which may become critical in the single-subject case. Contrary to the standard procedure used in group analysis, we thus perform atlas-to-subject registration rather than subjects-to-atlas warping. A careful registration procedure (described in section II-D) is devised, to map a high-resolution (HR) anatomical atlas on the low-resolution rs-fMRI signal. This procedure preserves both the fMRI signal and the (high) resolution of the atlas anatomical regions. For traditional source separation methods, the number of components $R$ is fixed *a priori* arbitrarly. The estimated components then constitute either functional networks or noise components that must be filtered *a posteriori*. In our approach, we propose to work at the scale of the anatomical regions extracted from the finely segmented atlas, and we assume that functional networks are composed of small anatomical regions. In this case $R$ represents the number of regions of the HR segmentation map. The contribution of the HR segmentation map in the unmixing method is twofold. First, it is used to provide an accurate initialisation for the sparse abundance matrix $\mathbf{A}$, based on the fractions of anatomical regions present in each voxel. Second, the HR atlas is also used as an important regulariser in the DL formulation, constraining the sparse structure of the abundance matrix $\mathbf{A}$ during optimization. The proposed single-subject DL formulation is presented in Section 2. In Section 3, the unmixing approach is assessed on a semi-real rs-fMRI dataset (with ground truth) obtained on a mouse. The experimental results clearly illustrate the benefit of integrating an HR anatomical atlas in the single-subject case.

## II. Dictionary learning formulation

In this section, the method followed to find timecourses related to anatomical regions is presented.

### A. Optimisation problem

Given the observation model (1), the following minimisation problem:

$$\min_{\mathbf{A},\mathbf{U}} \frac{1}{2}\|\mathbf{Y}-\mathbf{U}\mathbf{A}\ \|_F^2 \tag{3}$$

does not have a unique solution because of the joint estimation of $\mathbf{A}$ and $\mathbf{U}$, and the ill-posedness of the problem. In order to restrain the number of solutions, we introduce some standard constraints on matrix $\mathbf{A}$ such as the *positivity constraint* $\mathbf{A} \in \mathbb{R}^+$ and the *sum-to-one constraint* $\sum \mathbf{A}[.,i] = 1$, with $i = 1 : P$, as these are the proportions voxel by voxel. The form of matrix $\mathbf{A}$ is also constrained by the extra information from the HR segmentation obtained by the projection of the atlas: we know precisely which anatomical regions contribute to a given voxel, i.e. present a non zero proportion at this voxel. The unmixing problem is recast as:

$$\min_{\mathbf{A},\mathbf{U}} \frac{1}{2}\|\mathbf{Y}-\mathbf{U}\mathbf{A}\|_F^2+\frac{\mu_\sigma}{2}\|\mathbf{U}\|_F^2+\mathcal{I}_{\mathbb{R}^+}(\mathbf{A})+\mathcal{I}_{\tilde{\mathbf{A}}}(\mathbf{A})+\mathcal{I}_S(\mathbf{A}), \tag{4}$$

where the first term is the data fidelity term, the second term is a Tikhonov regularisation controlled by parameter $\mu_\sigma$ set to $10^{-4}$ to prevent bad conditioning(see section II-B). The third term is a positivity constraint where $\mathcal{I}_{\mathbb{R}^+}(\mathbf{A}) = \infty$ if at least one of the elements of $\mathbf{A}$ is negative, and 0 otherwise. The fourth term $\mathcal{I}_{\tilde{\mathbf{A}}}(\mathbf{A})$ is the indicator function on the set of matrices having a structure similar to matrix $\tilde{\mathbf{A}}$. This is a binary matrix where element $(\tilde{\mathbf{A}})_{r,i} = 1$ if the $r^{th}$ projected high resolution anatomical region of the atlas intersects the $i^{th}$ low resolution voxel, and 0 otherwise. This gives $\mathcal{I}_{\tilde{\mathbf{A}}}(\mathbf{A}) = \infty$ if at least one element of $\mathbf{A}$ is non-zero while it is zero in $\tilde{\mathbf{A}}$, and 0 otherwise. The last term in eq. (4) codes the *sum-to-one* constraint on each column of matrix $\mathbf{A}$. $\mathcal{I}_S(\mathbf{A}) = \infty$ if at least one column of $\mathbf{A}$ does not sum to one, and 0 otherwise.

Estimating jointly $\mathbf{U}$ and $\mathbf{A}$ in eq. (4) is a typical problem of dictionary learning. But, unlike conventional DL algorithms (eq. (2)), there is no sparsity regularisation term in the form of a $\ell_1$ penalty: it is the term $\mathcal{I}_{\tilde{\mathbf{A}}}(\mathbf{A})$ which enforces the sparse decomposition of each voxel. This underlines the importance of the HR segmentation map used to guide the fMRI data unmixing. A classical way to solve the joint estimation problem is to optimise alternatively the cost function eq. (4) along $\mathbf{U}$ and $\mathbf{A}$.

### B. Timecourse matrix estimation

Considering $\mathbf{A}$ is fixed, problem (4) becomes:

$$\min_{\mathbf{U}} \frac{1}{2}\|\mathbf{Y}-\mathbf{U}\mathbf{A}\ \|_F^2+\frac{\mu_\sigma}{2}\|\mathbf{U}\|_F^2. \tag{5}$$

Here the Tikhonov regularisation term $\mu_\sigma\|\mathbf{U}\|_2^2$ is not used to enforce temporal smoothness of columns of U but to improve the conditioning of the problem (3). In our case, $\mu_\sigma$ is set to $10^{-4}$ to prevent collinearity between columns of $\mathbf{A}$ without increasing timecourses smoothing. Such a situation may occur when two very thin neighbouring regions of the segmentation map are projected on the fMRI data. Since the fMRI data are of low spatial resolution, these two regions may project on exactly the same voxels, yielding collinearity. The solution of (5) is the ridge estimator defined by:

$$\hat{\mathbf{U}} = \mathbf{Y}\mathbf{A}^T(\mathbf{A}\mathbf{A}^T+\mu_\sigma\mathbf{I}_R)^{-1}, \tag{6}$$

where $\mathbf{I}_R$ is the $R \times R$ identity matrix.

### C. Abundance matrix estimation

Consider that $\mathbf{U}$ is fixed, then problem eq. (4) becomes $\min_{\mathbf{A}} f(\mathbf{A})$ where:

$$f(\mathbf{A})=\frac{1}{2}\|\mathbf{Y}-\mathbf{U}\mathbf{A}\|_F^2+\mathcal{I}_{\mathbb{R}^+}(\mathbf{A})+\mathcal{I}_{\tilde{\mathbf{A}}}(\mathbf{A})+\mathcal{I}_S(\mathbf{A}). \tag{7}$$

Note that this function is separable according to the voxels $i \in \{1,\ldots, \mathrm{P}\}$ which leads to: $\min_{\mathbf{a}_i} f(\mathbf{a}_i)$, with:

$$f(\mathbf{a}_i)=\frac{1}{2}\|\mathbf{y}_i - \mathbf{U}\mathbf{a}_i\|_F^2+\mathcal{I}_{\mathbb{R}^+}(\mathbf{a}_i)+\mathcal{I}_{\tilde{\mathbf{a}}_i}(\mathbf{a}_i)+\mathcal{I}_S(\mathbf{a}_i), \quad (8)$$

where $\mathbf{a}_i$ is a column vector from the matrix $\mathbf{A}$. The set of all the vectors with a structure similar to $\mathbf{a}_i$ is given by $\tilde{\mathbf{a}}_i$, where $\tilde{\mathbf{a}}_i$ is a column of $\tilde{\mathbf{A}}$. The regularisation terms in eq. (8) can be summarized as $g(\mathbf{a}_i) = \mathcal{I}_{\mathbb{R}^+(\mathbf{a}_i)\cap\tilde{\mathbf{a}}_i(\mathbf{a}_i)\cap S(\mathbf{a}_i)}$.

The convexity of the set $\mathbb{R}^+ \cap \tilde{\mathbf{A}} \cap S$ can be easily verified. Let us notice that eq. (8) belongs to the class of problems for which the proximal gradient method can be used. Different algorithms are available, for example, projected gradient, also known as iterative shrinkage-thresholding algorithm (ISTA) or FISTA (Fast ISTA) [11]. FISTA was preferred for its rapid convergence: its implementation is given in Algorithm 1.

**for** $k \leftarrow 1$ **to** $proxsteps$ **do**
  $\mathbf{a}_i^{(k)} = prox_g(\boldsymbol{\omega}^{(k)} - \lambda\nabla f(\boldsymbol{\omega}^{(k)}))$
  $t^{(k+1)} = \frac{1+\sqrt{1+4\left(t^{(k)}\right)^2}}{2}$
  $\boldsymbol{\omega}^{(k+1)} = \mathbf{a}_i^{(k)} + \left(\frac{t^{(k)}-1}{t^{(k+1)}}\right)(\mathbf{a}_i^{(k)} - \mathbf{a}_i^{(k-1)})$
**end**

**Algorithm 1:** FISTA algorithm for estimating columns $\mathbf{a}_i$ of matrix $\mathbf{A}$.

In algorithm 1, $\nabla f(\mathbf{a}_i)$ is the gradient of $f(\mathbf{a}_i)$, given by $\mathbf{U}^T(\mathbf{U}\mathbf{a}_i-\mathbf{y}_i)$. The step size $\lambda$ is set equal to the inverse of the Lipschitz constant of $\nabla f(\mathbf{a}_i)$ i.e. $1/L$, where $L = \|\mathbf{U}^T\mathbf{U}\|_F$, $t^{(k+1)}$ is an auxillary variable which helps in the fast convergence of FISTA, $\boldsymbol{\omega}$ calculates intermediate values based on a special linear combination of the last two points and $prox$ refers to the proximal operator [11]. In our case, the proximal operator is just the projection of $\mathbf{a}_i$ in the positive orthant, with the vector normalised *to-sum-to-one*. This projection also forces the solution to be non-zero only at positions where an atlas region projects on the voxel, with the $\mathcal{I}_{\tilde{\mathbf{a}}}$ constraint. The proximal operator of the function $g$ is:

$$prox_g(\mathbf{y}) = \underset{\mathbf{x}\in\mathbb{R}^+\cap\tilde{\mathbf{a}}_i\cap S}{\operatorname{argmin}} \|\mathbf{x}-\mathbf{y}\|_2 = \mathcal{P}_{\mathbb{R}^+\cap\tilde{\mathbf{a}}_i\cap S}(\mathbf{y}), \quad (9)$$

where $\mathcal{P}$ is the projection operator on the set $\mathbb{R}^+ \cap \tilde{\mathbf{a}}_i \cap S$. The orthogonal projection of a vector $\mathbf{y} \in \mathbb{R}^R$ on $\mathbb{R}^+ \cap \tilde{\mathbf{a}}_i \cap S$ is obtained using the projection onto convex sets (POCS) method [12]. POCS algorithm alternates projection onto the simplex $\mathbb{R}^+ \cap S$ and projection onto the set of vectors having the same structure as $\tilde{\mathbf{a}}_i$. Only a few iterations are required for convergence of the POCS algorithm.

Convergence towards a global minimum of DL algorithms cannot be proven. In practice, a good initialisation of $\mathbf{A}$ and the presence of pure pixels (as in remote sensing application) in each region guarantee a good joint estimation of $\mathbf{U}$ and $\mathbf{A}$.

### D. Initialisation of the algorithm and atlas registration

A good initialisation of $\mathbf{A}$ is required: to this end, information from the HR segmentation map is used. As already explained, the HR atlas is registered to the fMRI data. Note that instead of warping the atlas to the fMRI data, we register the atlas to the structural (anatomical) MR image (which is itself registered to the fMRI data), since structural MRI contains more spatial information than fMRI data. A problem we encountered is that the atlas has a much higher spatial resolution than the fMRI or structural MRI data (up to a factor of 20 in one of the dimensions). This large difference in resolution is not properly handled by the deformable registration methods used in medical imaging such as FLIRT [13] or ANTS [14]. To overcome this problem, the resolutions of fMRI and anatomic MRI data were artificially increased by subdividing their voxels in the 3 spatial dimensions until the same order of magnitude as the atlas resolution is achieved. A diffeomorphic deformable registration of the atlas to the resolution-augmented structural MRI is then performed with ANTS [14]. It provides an accurate projection of the HR atlas on the fMRI data, preserving the structure of thin regions.

Finally, DL is performed at the (low) resolution of the initial fMRI data $\mathbf{Y} \in \mathbb{R}^{N\times P}$. The initial abundance matrix $A^{(0)} \in \mathbb{R}^{R\times P}$ is constructed as follows. Let's say that each voxel $i \in \{1,\ldots, \mathrm{P}\}$ was subdivided into $J$ high resolution voxels during the artificial augmentation step. For each voxel $i$ of $\mathbf{Y}$ and all regions $r \in \{1,\ldots,R\}$, the element $(A^{(0)})_{r,i}$ will contain the proportion of high resolution voxels in voxel $i$, occupied by region $r$. If region $r$ is not transported to the low-resolution voxel $i$ then $(A^{(0)})_{r,i} = 0$.

## III. Application and Results

### A. Data and atlas

In order to test the proposed unmixing algorithm, we use data acquired in a preclinical study with an Alzheimer mice model. In this work, the data consist of a 4D rs-fMRI and a 3D anatomical image registered to the rs-fMRI image. The anatomical image has a dimension of $256 \times 256 \times 34$ and $0.08299 \times 0.07812 \times 0.4$ $mm$ resolution. Functional image has a dimension of $147 \times 87 \times 27 \times 500$ with $0.1445 \times 0.2299 \times 0.5$ $mm$ spatial resolution and 2s for the time resolution.

For initialising the abundance matrix $\mathbf{A}^{(0)}$ (see Section II-D), the mouse Allen Brain Atlas (ABA) is used [15]. ABA provides a 3D MRI volume (template) and a structural annotation volume, both at $25 \times 25 \times 25$ $\mu m$ resolution. The annotations consist of an HR segmentation map that identifies the different anatomical structures in the mouse brain.

### B. Atlas registration and fMRI preprocessing

The classical fMRI preprocessing pipeline of slice timing and co-registration is applied on the rs-fMRI data set. The next step consists in registering the spatially well-resolved ABA template to the artificially augmented anatomical image (which is perfectly aligned with the rs-fMRI data). The registration of the ABA mouse template to the anatomical images provides the deformation field that is applied to the HR segmentation map to transport the different labelled regions on the augmented rs-fMRI data. The spatial resolution of rs-fMRI data is augmented by subdividing each original voxel

into $3 \times 6 \times 2$ high resolution voxels. The registration of the anatomical image to the augmented rs-fMRI leads to an increase in its own resolution.

Confounding signals are regressed before analysing the data. A principal component analysis enables the isolation of hypersignal due to the presence of liquid in ventricles and of perturbations due to the interleaved acquisition. Regressed rs-fMRI data are then temporally standardised and used in the following processing.

### C. Validation data set

For validating the contribution of the HR segmentation map in unmixing the single-subject fMRI data, a set of synthetic temporal signatures are introduced in seven small regions arbitrarily chosen in the prefrontal cortex. A first synthetic signal is obtained by averaging the signals of the regions ACAd1 and ACAd5 which were already highly correlated in the real data. This signal is then modified to create signals with arbitrary high correaltion or anti-correlation for the regions ACAd1, ACAd5, ACAd6a, ACAv1, ACAv5, ORBl1 and PL1 (see blue lines in plots of figure 2). These correlations don't have a physical significance, they are used as a ground truth for evaluation of the proposed algorithm performances. Their correlations are presented in Table I.

| | ACAd1 | ACAd5 | ACAd6a | ACAv1 | ACAv5 | PL1 | ORBl1 |
|---|---|---|---|---|---|---|---|
| ACAd1 | 1.00 | 0.84 | 0.92 | 0.67 | 0.69 | -0.45 | -0.59 |
| ACAd5 | 0.84 | 1.00 | 0.92 | 0.67 | 0.69 | -0.47 | -0.60 |
| ACAd6a | 0.92 | 0.92 | 1.00 | 0.66 | 0.67 | -0.46 | -0.58 |
| ACAv1 | 0.67 | 0.67 | 0.66 | 1.00 | 0.88 | -0.59 | -0.82 |
| ACAv5 | 0.69 | 0.69 | 0.67 | 0.88 | 1.00 | -0.60 | -0.82 |
| PL1 | -0.45 | -0.47 | -0.46 | -0.59 | -0.60 | 1.00 | 0.74 |
| ORBl1 | -0.59 | -0.60 | -0.58 | -0.82 | -0.82 | 0.74 | 1.00 |

TABLE I: Correlation values between the seven synthetic temporal signatures introduced in the real data set.

Synthetic signals are introduced in the standardized artificially augmented fMRI data, which are then reduced to the initial low resolution. These synthetic signals are thus mixed with the real signals in the voxels containing a portion of the seven selected regions.

### D. Data unmixing results

The proposed DL method guided by the HR segmentation map is applied to the validation data set. Figure 1a shows the correlation between the temporal signatures of the seven synthetic regions and their neighbours in the prefrontal cortex after 500 iterations for estimating $\mathbf{A}$ and $\mathbf{U}$. Empirically, the algorithm allows convergence to an acceptable solution for $\mathbf{A}$ and $\mathbf{U}$. After 500 iterations, the gain on minimization of problem (4) is very low ($< 10^{-3}$). For the estimation of $\mathbf{A}$, the FISTA algorithm requires a stopping criterion or a maximum number of iterations. In our implementation, FISTA is stopped when $\|\mathbf{a}_i^{(k-1)} - \mathbf{a}_i^{(k)}\| < 10^{-8}$ or $k > 100$.

To highlight the crucial contribution of a well-registered HR segmentation map, we have applied the standard ANTS registration algorithm to the validation dataset, without handling the augmentation of resolution. The ABA template is thus directly registered on the low-resolution anatomical image using ANTS (initialisation of $\mathbf{A}^{(0)}$ is straightforward in this case). Figure 1b shows the correlation matrix obtained in this case, after 500 iterations. The inaccurate initial projection of the different anatomical structures on the low resolution fMRI data yields a poor initialization $\mathbf{A}^{(0)}$ for the abundance matrix. This results in a correlation matrix in figure 1b where the estimated correlations are far away from the ground truth.

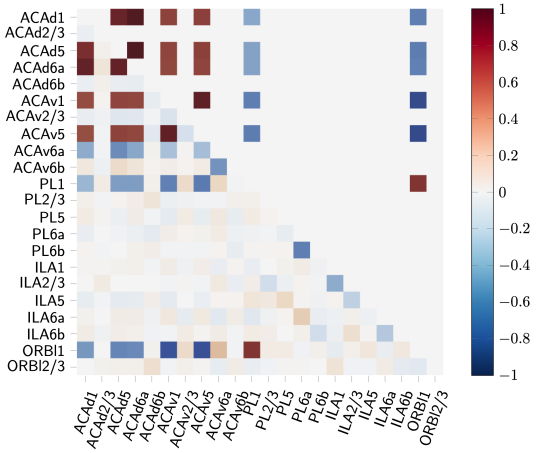


(a) DL algorithm guided by HR segmentation map

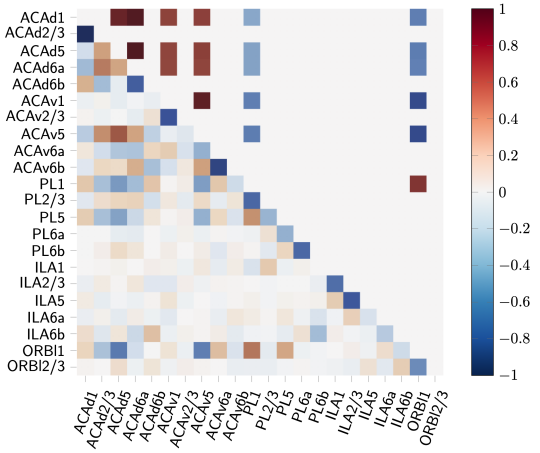


(b) Without HR registration

Fig. 1: Correlations in the prefrontal cortex. The lower triangular matrix contains estimated correlation and the upper triangular matrix contains the true ones for the seven synthetic signatures. Diagonal elements are set to zero.

Figure 2 shows the synthetic signals introduced (in blue), the estimated timecourses with information from the HR atlas (in dashed red) and the estimated timecourses without the contribution of the information from the HR atlas (in green). The mean square error (MSE) of the estimated timecourses have been shown on the plots. It can be seen that the MSE(HR), which contains information from the high resolution atlas, have values significantly lower than the MSE without the extra information.

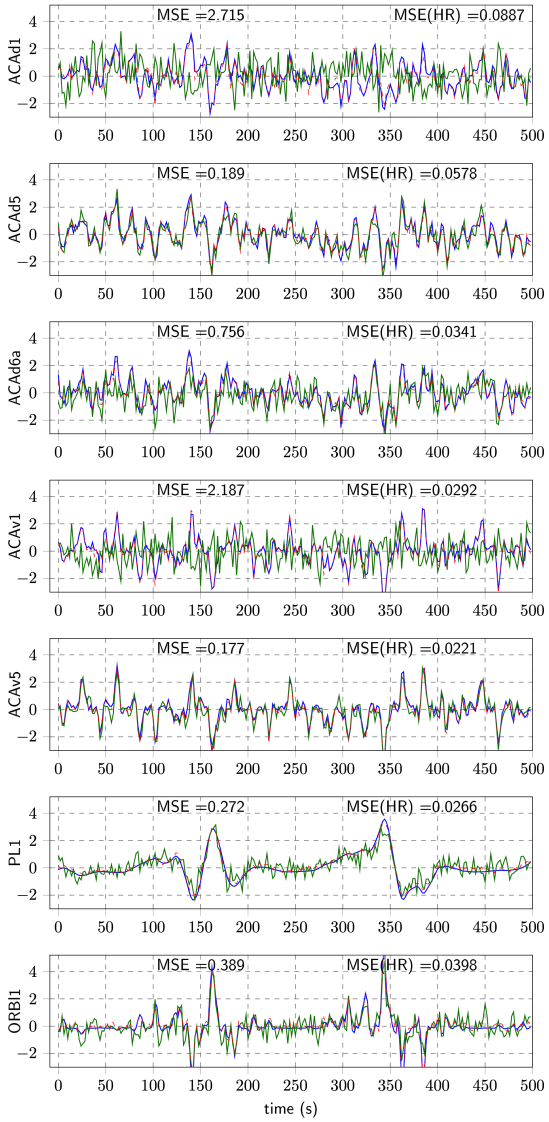


Fig. 2: The plot shows samples corresponding to the first 500 seconds of the synthetic signals (in blue) and their corresponding estimated timecourses using HR altas information (in dashed red) and without using HR atlas information (in green).

### *E. Discussion*

Unmixing algorithms are often sensitive to the assumption of pure pixels (i.e. each region has an abundance of 1 in at least one pixel of the image). Since the HR ABA template provides a (very) fine segmentation of thin brain structures, this assumption is not guaranteed once the regions are projected onto the low resolution fMRI data. In order to challenge this hypothesis, additional synthetic data were simulated. In a first case, a region was completely included in another region and in a second case, a region was superimposed on two or more regions. In the first case, it was difficult to correctly estimate the timecourse of the region included in the other (and therefore its abundance). In the second case, the timecourse is better estimated and so is its abundance. In practice, the first case should not occur in fMRI data, which ensures that we can correctly estimate both the abundances and the timecourses.

## IV. Conclusion

The choice to register the HR atlas to the fMRI data for preserving the timecourses from any interpolation led us to introduce new constraints in the DL formulation. These constraints carefully exploit the HR segmentation map to initialize and estimate the abundance matrix. This unmixing method can be used for other applications, such as remote sensing or astronomy, as long as it is possible to register an HR segmentation map on the low-resolution data set. The next step is the timecourses analysis that can be carried out by multifractal [16] or spectral analysis.

## References


[1] M. H. Lee, C. D. Smyser, and J. S. Shimony, "Resting-state fmri: a review of methods and clinical applications," *American Journal of Neuroradiology*, vol. 34, no. 10, pp. 1866–1872, 2013.

[2] N. K. Logothetis and B. A. Wandell, "Interpreting the bold signal," *Annu. Rev. Physiol.*, vol. 66, pp. 735–769, 2004.

[3] V. Zerbi, J. Grandjean, M. Rudin, and N. Wenderoth, "Mapping the mouse brain with rs-fmri: An optimized pipeline for functional network identification," *NeuroImage*, vol. 123, pp. 11 – 21, 2015. [Online]. Available: http://www.sciencedirect.com/science/article/pii/S1053811915007399

[4] J. P. Owen, Y.-O. Li, F. G. Yang, C. Shetty, P. Bukshpun, S. Vora, M. Wakahiro, L. B. Hinkley, S. S. Nagarajan, E. H. Sherr *et al.*, "Resting-state networks and the functional connectome of the human brain in agenesis of the corpus callosum," *Brain connectivity*, vol. 3, no. 6, pp. 547–562, 2013.

[5] A. Hyvärinen and E. Oja, "A fast fixed-point algorithm for independent component analysis," *Neural Comput.*, vol. 9, no. 7, pp. 1483–1492, Oct. 1997. [Online]. Available: http://dx.doi.org/10.1162/neco.1997.9.7.1483

[6] V. G. van de Ven, E. Formisano, D. Prvulovic, C. H. Roeder, and D. E. Linden, "Functional connectivity as revealed by spatial independent component analysis of fmri measurements during rest," *Human brain mapping*, vol. 22, no. 3, pp. 165–178, 2004.

[7] V. D. Calhoun and T. Adali, "Unmixing fmri with independent component analysis," *IEEE Engineering in Medicine and Biology Magazine*, vol. 25, no. 2, pp. 79–90, 2006.

[8] A. Abraham, E. Dohmatob, B. Thirion, D. Samaras, and G. Varoquaux, "Extracting brain regions from rest fmri with total-variation constrained dictionary learning," in *International Conference on Medical Image Computing and Computer-Assisted Intervention*. Springer, 2013, pp. 607–615.

[9] H. Eavani, R. Filipovych, C. Davatzikos, T. D. Satterthwaite, R. E. Gur, and R. C. Gur, "Sparse dictionary learning of resting state fmri networks," in *Pattern Recognition in NeuroImaging (PRNI), 2012 International Workshop on*. IEEE, 2012, pp. 73–76.

[10] G. Varoquaux, A. Gramfort, F. Pedregosa, V. Michel, and B. Thirion, "Multi-subject dictionary learning to segment an atlas of brain spontaneous activity," in *Information Processing in Medical Imaging*. Berlin, Heidelberg: Springer Berlin Heidelberg, 2011, pp. 562–573.

[11] A. Beck and M. Teboulle, "A fast iterative shrinkage-thresholding algorithm for linear inverse problems," *SIAM Journal on Imaging Sciences*, vol. 2, no. 1, pp. 183–202, 2009.

[12] S. Boyd, J. Dattorro *et al.*, "Alternating projections," *EE392o, Stanford University*, 2003.

[13] M. Jenkinson, P. Bannister, M. Brady, and S. Smith, "Improved optimization for the robust and accurate linear registration and motion correction of brain images," *Neuroimage*, vol. 17, no. 2, pp. 825–841, 2002.

[14] B. B. Avants, N. Tustison, and G. Song, "Advanced normalization tools (ANTS)," *Insight Journal*, vol. 2, pp. 1–29, 2009.

[15] S. W. O. et al., "A mesoscale connectome of the mouse brain," *Nature*, vol. 508, pp. 207–214, 2014.

[16] D. M. Cole, S. M. Smith, and C. F. Beckmann, "Advances and pitfalls in the analysis and interpretation of resting-state fmri data," *Frontiers in systems neuroscience*, vol. 4, p. 8, 2010.